ESAIM: PROCEEDINGS, August 2009, Vol. 28, p. 135-149
M. Ismail, B. Maury & J.-F. Gerbeau, Editors

DRY GRANULAR FLOWS WITH EROSION/DEPOSITION PROCESS *

C.-Y. Kuo[1], B. Nkonga[2], M. Ricchiuto[3], Y.-C. Tai[4] and B. Braconnier[5]

Abstract. In this work we use the erodible model proposed by Tai and Kuo [18] to investigate complex granular flows in which deposition and erosion are significant. The initial motivation comes from experiments of granular collapse which exhibit both phenomena. A numerical model with a flux balanced scheme is developed, and the eigenstructure of its quasilinear form as well as the entropy inequality are assessed. Numerical application is performed for granular column collapse is simulated by the new well-balanced scheme. For the latter, numerical results demonstrate an upward evolution of the interface between the flowing layer and stagnant base. Comparison between the numerical and the experimental data not only illustrates the advantages of this model of erosion/deposition mechanisms but also reveals the future directions for further study.

Résumé. Ce travail consiste à utiliser un modèle proposé par Tai and Kuo [18], pour étudier un écoulement granulaire sec, dans lequel l'érosion et la déposition jouent un rôle très important. Cette étude est motivée par des expériences d'effondrement d'une colonne de sable, qui montrent la coexistence des ces deux phénomènes physiques. Une approche numérique consistante et préservant certaines asymptotiques est étudiée et mise en $\frac{1}{2}$uvre. Les résultats numériques sont globalement cohérents aux expériences. Néanmoins, ils révèlent aussi les limites de l'actuelle modélisation du mécanisme d'érosion/déposition et suggèrent de futures investigations.

1. Introduction

In recent years, the study of granular media has received a great attention from mechanicists in both natural environment and industrial application fields. Depending on the flow states, the granular medium can exhibit both solid and fluid behaviors. Thus, it is a challenging task to understand its dynamics, and to propose sufficiently accurate models. Nevertheless, progress has been made. For granular media behaving as a fluid, such as avalanche flows down inclined planes, PDEs similar to the shallow water equations have been derived in e.g. Savage and Hutter (1989) [1], Mangeney-Castelnau et al. (2005) [10]. Applications of such models and their comparison with experiments are reviewed in Pudasaini and Hutter (2007) [2].

In the aforementioned systems, the basal bottom is assumed fixed, i.e. the variation of the basal surface is assumed to be minor and negligible. However, in many natural landslides the flow behavior is greatly influenced

* *This work is supported by a French/Taiwan program ORCHID: Grant of the National science council (Taiwan) and EGIDE (France)*

[1] Academia Sinica (Taiwan), cykuo06@gate.sinica.edu.tw

[2] Nice Sophia-Antipolis univ. (France), nkonga@unice.fr

[3] INRIA Bordeaux Sud-Ouest(France), mario.ricchiuto@inria.fr

[4] Chi Nan Univ (Taiwan), yctai@ncnu.edu.tw

[5] GLAIZER group innovation agency (France), benjamin.braconnier@glaizer.com

Article published by EDP Sciences and available at http://www.edpsciences.org/proc or http://dx.doi.org/10.1051/proc/2009043

by the erosion/deposition process. Due to the complexity of this mechanism, an appropriate continuum mechanics model has necessarily to rely on experimental data. A key experiments to understand the erosion/deposition mechanisms is the collapse of a granular column, in which the flow exhibits both erosion and deposition. Lajeunesse et al. (2004) [11] and Lube et al. (2004) [12] studied the axi-symmetric collapse of granular columns and showed that the major governing parameter is the aspect ratio, defined as the ratio of the initial height to the initial radius of the column. Lube et al. (2005) [13] further investigated the collapses of a two-dimensional granular column and found that the collapse time varies as the square root of the initial column height but it is independent of its width. Around the same time, work on two-dimensional granular collapses was also performed by Balmforth and Kerswell (2005) [14]. Thompson and Huppert (2007) [15] considered instead the collapse of initially saturated sand piles into quiescent water. In addition to experimental measurements, both continuum and discrete models have been employed. For example, Staron and Hinch (2005) [16] simulated the two-dimensional collapse using a discrete-grains method, and Mangeney et al. (2006) [17] compared the two continuum shallow-water type models for granular spreading. Of the above mentioned studies, only few have actually investigated the internal structure of the collapse, i.e. the interaction between the flowing layer and the basal resting granular media. This interaction is dominated by the erosion/deposition mechanisms taking place during the collapse.

The aim of this study is to gain a better understanding of the details of the internal structure of the granular column collapse by both theoretical modeling and comparison with experimental observations. In the first section of the paper, we describe an experimental set up and associated observations of the erosion/deposition process. Then we consider the 1D mathematical model proposed Tai and Kuo [18], and discuss some of its properties. We propose a finite volume scheme able to preserve conservations properties and some natural asymptotics of the model (well balanced).

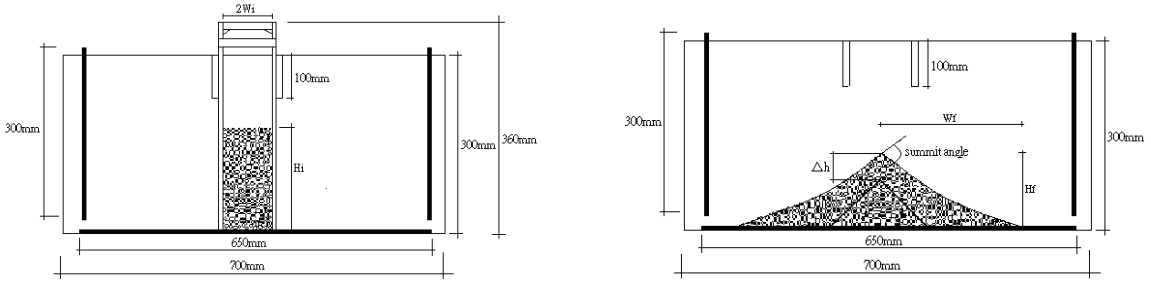

FIGURE 1. Initial setup for the experiment with a rough sketch of the final deposit beneath [22].

2. Experimental setup and investigations

The experimental observations we performed aim at measuring the spreading of a finite mass of dry granular column suddenly released on a horizontal plane. The use of a high-speed digital camera and image processing tools, allow to highlight the existence of an internal stagnant core, as well as the evolution of the flowing layer. To improve the quality of the observations, the granular mass (Ottawa sand) was dyed into alternative layers of different colors. These observations show the existence of a bell (or triangular) shaped region inside which the grains are not affected by the collpase from its initiation to the final deposit. This means that a surface flow is developed in the collapse column along its edges while a static bulk remains at its core. Another interesting feature is that the higher layer progressively covers the lower one, which leads to the stratification on both sides.

Fig. 1 illustrates the experimental setup, where the granular materials are confined between two glass sheets 8 mm thick at an internal width 19 mm. The vertical column of granular mass is confined by a confinement handlebar. Once the confinement handlebar is suddenly released, the vertical column of granular grains begins to spread on both sides. Initially, right after the release of the confinement, the grains fall almost vertically onto

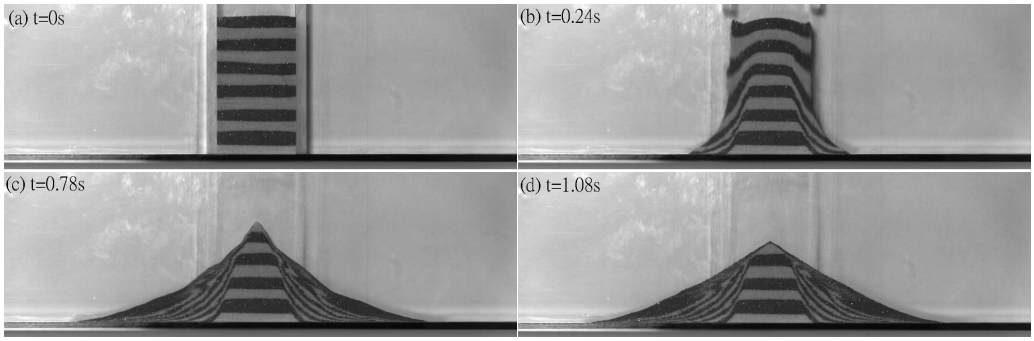

FIGURE 2. Spreading of the granular column (Ottawa snad 30-50, $\mathrm{H_i} = 132$ mm, $\mathrm{W_i} = 40$ mm) [22].

the lower section, and are deflected outwards. The foothill corners are then smoothed. As a consequence of this smoothing, the grains flow down over the surface of the deposit in form of surface flows which gradually become thinner as time elapses. When the flow stops, a final deposit of conical shape is obtained. In the following, we shall use the same notations introduced in some of the author's earlier works (e.g. [12], [17] or [15]). In particular, the initial width and height of the granular column are denoted as $2\mathrm{W_i}$ and $\mathrm{H_i}$, respectively, whilst the final width and height of the deposit are expressed by $2\mathrm{W_f}$ and $\mathrm{H_f}$, respectively. In experiments the initial width of the column is $2\mathrm{W_i} = 80$ mm and $\mathrm{H_i} = 132$ mm, which implies the aspect ratio ($a = \mathrm{H_i}/\mathrm{W_i} = 3.3$).

Figure 2 illustrates the sequence of images corresponding to Ottawa sand 30-50 ($d = 0.6-0.85$ mm) spreading on a steel plane. The initial column is dyed into alternative layers of light brown and black colors, as it can be seen in Fig. 2_a. Subsequent figures, Figs. 2_b and 2_c show the vertical side flows immediatly after the release and the resultant stratified topographical base (with a thin layer of surface flow). Once the fina deposit is obtained, Fig. 2_d, one clearly sees that a region of the granular mass inside a bell-shaped core is not affected by the flow. In addition, due to the surface flows when the column collapses, we observe the stratification on both sides. This quasi-two-dimensional collapse has two major features different from the axi-symmetrical three-dimensional experiments conducted by Lajeunesse et al. (2004) [11], in which the granular column is released by a tube: first, the internal non-affected core is of a bell-shape rather than a wedge-shape as in [11] and, second, the stratification is not present in earlier observations.

3. Mathematical model and analysis

In the present work, a simple erosion/deposition rate is adopted (see TK 2008 for details of the mathematical derivation). It is derived from Bouchaud et al.[3] but with a minor modification: the value of erosion/deposition rate is proportional to the thickness of the flowing layer, and to the difference between the topographic inclination angle and the angle of repose. This dependence on the thickness can equally be interpreted as a dependence on the pressure perpendicular to the sliding surface. This is likely the more adequate interpretation because it is a "local"effect. In addition, based on experimental observation, a threshold speed, corresponding to a threshold kinetic energy, is introduced. This allows to model tha fact that the deposition procedure takes place only when the local speed is less than some threshold speed.

3.1. **Terrain-following coordinate**

Let $\boldsymbol{x}$ denote the Cartesian coordinates, in which the x-axis lies on the horizontal plane and the z-axis points upwards in the vertical direction (see Fig. 3). On the topographic surface one can define curvilinear coordinates $\boldsymbol{\xi} \in \mathbf{R}^2$, where the component ξ is on the terrain surface and ζ lies in the normal direction. If the parametrization of the topographic surface $F(t, x, z) = z - b(t, x) = 0$ is given and assumed to be sufficiently

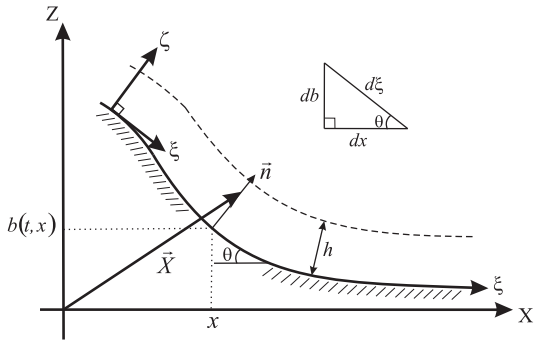

FIGURE 3. Bijection between the Cartesian ($\boldsymbol{x}$) and curvilinear ($\boldsymbol{\xi}$) coordinates [18].

smooth and differentiable, its unit normal vector is then given by

$$\boldsymbol{n} = c \begin{pmatrix} -\partial_x b, \\ 1 \end{pmatrix} = \begin{pmatrix} -s \\ c \end{pmatrix}, \tag{1}$$

where $c = (1 + (\partial_x b)^2)^{-1/2}$ and $\partial_x b$ is the topographic derivative with respect to the horizontal coordinate x. With the help of (1) we can decompose any point within the flowing layer above the topographic surface as

$$\boldsymbol{x} = \begin{pmatrix} x \\ z \end{pmatrix} = \begin{pmatrix} x \\ b \end{pmatrix} + \zeta \boldsymbol{n}, = \begin{pmatrix} x \\ b \end{pmatrix} + \zeta \begin{pmatrix} -s \\ c \end{pmatrix} \tag{2}$$

where the first term on the right-hand side is the Cartesian basal reference and the second term is the local depth in a sense normal to the basal surface. Letting θ be the local inclination angle measured from the horizontal (see Fig. 3), the local curvature κ_1 is then given by $\kappa_1 = (\partial_x s) = (c^3 \partial_{xx} b) = -(\partial\theta/\partial\xi)$. As long as ζ is locally smaller than the radius of curvature of the basal curve, expression (2) uniquely defines a position vector in both $\boldsymbol{x}$- and $\boldsymbol{\xi}$-coordinates.

To cope with variable topographic surfaces, the $\boldsymbol{\xi}$-coordinate is generalized to include a temporal variable τ. Then by virtue of the Unified Coordinate (UC) method ([5,6], [7,8]), the variables in $\boldsymbol{\xi}$-coordinates, (τ, ξ, ζ), can be obtained via a transformation from the Cartesian coordinates, (t, x, z), by

$$\begin{cases} dt \;=\; d\tau \,, \\ d\boldsymbol{x} = \boldsymbol{q}\, d\tau + \underline{\boldsymbol{F}}\, d\boldsymbol{\xi} \,. \end{cases} \tag{3}$$

Here $\boldsymbol{q}$ denotes the velocity of the coordinate in $\vec{X}$-coordinates, and $\underline{\boldsymbol{F}} = \frac{\partial \boldsymbol{x}}{\partial \boldsymbol{\xi}}$ is the Jacobian matrix of transformation of the two coordinate systems. With the definition, $D_{\boldsymbol{q}} \equiv \partial_t + \boldsymbol{q}\partial_{\boldsymbol{x}}$, and by virtue of (3), it is obvious that $D_{\boldsymbol{q}}\boldsymbol{\xi} = 0$, i.e., ($\xi$, ζ) can be thought to be the position of a pseudo-particle of velocity $\boldsymbol{q}$. Thus, by requiring that the coordinate moves along with the moving surface of the physical system it implies that the ξ-axis, $\zeta = 0$, will always coincide with the topography surface, whether erosion or deposition takes place.

3.2. **Field equations**

We denote by $\boldsymbol{q}$ and $\boldsymbol{q}^*$ the particle velocities in the $\boldsymbol{x}$- and $\boldsymbol{\xi}$-coordinates, respectively:

$$\boldsymbol{q} = \begin{pmatrix} u \\ w \end{pmatrix}, \quad \boldsymbol{q}^* = \begin{pmatrix} q_\xi \\ q_\zeta \end{pmatrix},$$

Namely, u and w are the horizontal and vertical velocity components, respectively, whilst, q_ξ and q_ζ are the velocity components parallel to the ξ- and ζ-coordinates. With the assumptions of *(i) approximately uniform distribution of the velocity through the thickness and (ii) shallow curvature and geometry of the flowing body*, the leading-order depth-integrated non-dimensional equations of mass and momentum balances are

$$\frac{\partial h}{\partial \tau} + \frac{\partial}{\partial \xi}\big(h q_\xi\big) = -\mathcal{E} \ , \tag{4}$$

$$\frac{\partial (hu)}{\partial \tau} + \frac{\partial}{\partial \xi}\left(h u q_\xi + \frac{\beta_\xi h^2}{2}\right) = -\mathcal{E} u + h\mathcal{S} \ , \tag{5}$$

where h is the depth of the flow and $\mathcal{E}$ is the volume flow through the basal surface at the density of the flow. In the above equations, u is the mean value of the horizontal velocity component, q_ξ is the mean velocity component parallel to the ξ-coordinate. The factor β_ξ, containing the behavior of the Mohr-Coulomb material, is

$$\beta_\xi = \beta(q_\xi, \theta) = \mathcal{K}(q_\xi)\cos^2\theta \ , \tag{6}$$

$\mathcal{K}(q_\xi)$ is the so-called earth pressure coefficient is determined by (Savage and Hutter [1])

$$\mathcal{K}(q_\xi) = \begin{cases} K_- & \text{if } \frac{\partial q_\xi}{\partial \xi} \geq 0 \\ K_+ & \text{else} \end{cases} \qquad \text{where } \ K_\pm = \frac{2H}{L}\left(\frac{1 \pm \sqrt{1 - cos^2\varphi/\cos^2\delta}}{\cos^2\varphi} - \frac{1}{2}\right) \tag{7}$$

where H and L are typical avalanche height and its extent parallel to the bed, ϕ and δ are respectively the internal and basal angles of friction specific to the considered granular material. The term $\mathcal{S}$ represents the net driving acceleration, including both the gravity acceleration and the sliding friction,

$$\mathcal{S} = \frac{N_b}{h}\Big(\sin\theta - \mu\,\epsilon^\beta\,\mathrm{sgn}(q_\xi)\,\cos\theta\Big) \ , \quad \text{with} \quad N_b = h\,\cos\theta + \epsilon^\alpha\, h\,\left(q_\xi\kappa_2 + q_\xi^2\kappa_1\right) \ , \quad \text{and} \quad \epsilon = \frac{H}{L}. \tag{8}$$

N_b is the normal pressure at the basal surface, μ $(= \tan\delta)$ is the basal friction coefficient. The first term on the right-hand side of N_b is the hydrostatic pressure, the second term is due to the temporal varying inclination angle, and the third one represents the influence of the centripetal acceleration towards the curvature center. The coefficient κ_1 denotes the local curvature, and κ_2 represents the time derivative of the negative local inclination angle $\kappa_2 = -\partial_\tau\theta$. Parameters α and β are data of the modelization, presumed [18] to lay in $]0,\ 1[$.

The non-dimensional variables in the above equations, (4) to (8) , can be mapped back to their physical counterparts (with tilde-mark) by applying the scalings,

$$\tilde{\xi} = L\,\xi \ , \quad (\tilde{q}_\xi,\, \tilde{\mathcal{E}}) = \sqrt{gL}\,(q_\xi,\, \epsilon\,\mathcal{E}) \ , \quad \tilde{N}_b = gH N_b \ , \quad \tilde{\tau} = \tau\sqrt{L/g} \ , \quad \tilde{\kappa}_1 = \kappa_1/\mathcal{R} \ , \quad \tilde{\kappa}_2 = \kappa_2\sqrt{gL}/\mathcal{R} \ , \tag{9}$$

where g is the gravitational acceleration, $\mathcal{R}$ is a typical radius of curvature of the topographic surface, κ_1 denotes the local curvature and κ_2 represents the time derivative of the negative local inclination angle.

3.3. **Erosion/deposition rate**

Following Bouchaud et al. [3], with a slight modification based on experimental observations, Tai and Kuo [18] suggested a model for the deposition rate $\mathcal{E}$ (negative erosion rate of the basal surface, different to the term $\mathcal{E}$ in (4) and (5), please refer to (12) for their relation) to describe the evolution of the variable basal surface. Relative to the neutral angle θ_n (the angle of repose of the material) three states exist

$$\begin{cases} \theta < \theta_n \text{ and } |q_\xi| > v_{th} \ \Rightarrow \ \mathcal{E} = 0 \ : \ \text{neither deposition nor erosion} \ , \\ \theta < \theta_n \text{ and } |q_\xi| < v_{th} \ \Rightarrow \ \mathcal{E} > 0 \ : \ \text{deposition} \ , \\ \theta > \theta_n \qquad\qquad\quad \Rightarrow \ \mathcal{E} < 0 \ : \ \text{erosion} \ . \end{cases} \tag{10}$$

Here, θ is the local inclination angle and v_{th} is the threshold speed, corresponding to a threshold kinetic energy for deposition. Explicitly, erosion occurs when the inclination angle is larger than the angle of repose, whilst deposition only takes place once the inclination angle is less than the angle of repose and the kinetic energy is less than the threshold. The threshold value could depend non-linearly on the property of the contact surface between the material and the static bed, or on the local inclination angle or on the local sliding surface, and on other parameters. Since more detailed experimental data is still missing, the threshold speed is chosen, following [18], by the *ad hoc* relation,

$$v_{th} = \alpha_v(\theta - \theta_n)^2 \ , \tag{11}$$

with an empirical parameter α_v. This relation implies that v_{th} depends on the square of the difference between the inclination angle and the neutral angle (of repose).

Since there is normally a density difference between the flowing layer and the stationary bottom underneath, with the aid of the jump condition of mass, one can obtain the relation of the deposition rate and volume loss rate $\mathcal{E}$ in (4) and (5),

$$\mathcal{E} = \frac{\rho}{\rho_+}\partial_\tau b = \alpha_\rho\, \partial_\tau b \ , \tag{12}$$

where α_ρ is the ratio of the density, ρ, of the flowing layer to the density, ρ_+, of the bottom. Following [18], the normal component of the coordinate velocity q_ζ is selected to be equal to the value of the deposition rate $\mathcal{E}$, i.e., $q_\zeta = \mathcal{E}$, and the tangential component q_ξ is selected to be zero, so that the ξ-axis ($\zeta = 0$) always coincides with the topographic surface.

As $h \to 0$, Andreotti et al. [9] proposed a trapping height H_{trap} below which the effective friction coefficient jumps to a larger value. In this sense, the deposition rate is proposed to be a function of the corrected thickness and difference between the inclination angle and neutral angle,

$$\partial_\tau b \simeq \alpha_e \left(h + \alpha_h\sqrt{h}\right)\sin(\theta_n - \theta)\left[f_{reg}\,\mathcal{H}(\theta_n - \theta) + \mathcal{H}(\theta - \theta_n)\right] \ , \tag{13}$$

$$\text{with} \quad f_{reg} = \tfrac{1}{2}\left(1 - \tanh\left[e_\alpha\left(|q_\xi| - v_{th}\right)\right]\right)$$

where h is the local thickness of the flowing layer measured perpendicular to the instantaneous basal surface. The coefficient α_h is an adjustment and could be a function of the size, or shape of the particle or the density ratio α_ρ. The coefficient α_e is an empirical rate factor and $\mathcal{H}(\bullet)$ is the Heaviside step function. The term f_{reg} is a function of the velocity q_ξ. The speed of the transition erosion/deposition is paramtrized by e_α.

The model just recalled has several advantages, related to both the dynamics of deposition, and the numerical simulation. First, the field equations are written in a curvilinear coordinate system and systematically include the curvature of the temporally varying basal topography. Thus, they are able to describe granular flows over a non-uniformly curved bed of general type, and the meshes are automatically fit the moving topography. Second, in contrast to the traditional description of governing equations over a moving coordinate (e.g., [4]), the physical quantity hu computed in (5), is expressed in the Cartesian coordinates. This fact avoids the complicated calculation of Christoffel symbols and computations of changing coordinate orientation. Third, the deposition processes take place when the flowing body is close to a state of rest. Through the introduction of the criterion (10) the angle of repose and a convex shape of the slope by the deposition heap can be well reproduced. Last, since a state of rest is available, the maximum run-out distance and duration of motion can be well determined.

4. Analysis of the one-dimensional model

In one dimension, we recast the model in the following compact form :

$$\partial_\tau \mathbf{w}(\tau, \xi) + \partial_\xi \mathbf{f}(\mathbf{w}, \theta) = \mathbf{\Sigma}(\mathbf{w}, \theta) \tag{14}$$

where

$$\mathbf{w} = \begin{pmatrix} h \\ hu \end{pmatrix} \quad \mathbf{f} = \begin{pmatrix} hq_\xi \\ huq_\xi + \beta(q_\xi,\theta)\dfrac{h^2}{2} \end{pmatrix} \quad \mathbf{\Sigma} = \begin{pmatrix} -\alpha_\rho \partial_\tau b \\ -\alpha_\rho u \partial_\tau b + h\mathcal{S}(u,\theta) \end{pmatrix} \tag{15}$$

with

$$q_\xi = \alpha_{q_\xi} u\,, \qquad \alpha_{q_\xi} = \frac{1}{\cos\theta}, \qquad \beta(q_\xi,\theta) = \mathcal{K}(q_\xi)\cos^2\theta = \frac{\mathcal{K}(q_\xi)}{\alpha_{q_\xi}^2}$$

Due to the relations $dx = \cos\theta d\xi$ and $\tan\theta = -\partial_x b$, the friction $h\mathcal{S}$ can be recast as

$$h\mathcal{S} \simeq -h\cos\theta\partial_\xi b - \mathrm{sign}(u) h\cos^2\theta\mathcal{N}(u) \quad \text{with} \quad \mathcal{N}(u) = \mu\epsilon^\beta\left[1 + \epsilon^\alpha\left(ua_0 + u^2 a_1\right)\right] \tag{16}$$

where $a_0 = \frac{\kappa_2}{\cos^2\theta}$ and $a_1 = \frac{\kappa_1}{\cos^3\theta}$. This expression highlights the dependence of the source term on the right hand side on the spatial variation of the basal surface b. In particular, we can immediately see that a steady solution with $u = 0$ (hence $\mathrm{sign}(u) = 0$) is characterized by the balance

$$\mathcal{K}_0 h\cos\theta\partial_\xi(h\cos\theta) + h\cos\theta\partial_\xi b = 0$$

where $\mathcal{K}_0 = \mathcal{K}(q_\xi = 0)$. This immediately leads to the following result.

Proposition 1. Model (14) admits the steady *lake at rest*-type solution

$$\mathcal{K}_0 h\cos\theta + b = C_h\,, \qquad u = 0$$

with $\mathcal{K}_0 = \mathcal{K}(0)$, and C_h a constant .
Denoting by $\eta(\tau,\xi) = b(\tau,\xi) + h(\tau,\xi)\cos\theta(\tau,\xi)$ the *free surface* of the material, if $\mathcal{K}_0 = 1$ we recover exactly the physical lake at rest condition

$$\eta = b + h\cos\theta = C_h$$

4.1. **Quasilinear form and eigenstructure**

To gain further insight into the model, and eventually derive upwind discretizations, we consider here the study of its quasi-linear form. In particular, we are interested in determining an eigen-decomposition of the jacobian of the flux $\mathbf{f}$ with respect to the state vector $\mathbf{w}$. In order to do this, we consider a physical state of *frozen erotion/deposition* in which the basal surface is fixed and the coefficients α_{q_ξ} and $\mathcal{K}$ are independent on the solution. This is summarized by the following hypothesis.

Hypothesis 1. For frozen erotion/deposition and fixed basal surface the model parameters α_{q_ξ} and $\mathcal{K}$ are independent of the unknown $\mathbf{w}$. We assume $\alpha_{q_\xi} = \alpha_{q_\xi}(\tau,\xi)$, and $\mathcal{K} = \mathcal{K}(\tau,\xi)$. In particular, we have

$$\partial_{\mathbf{w}}\alpha_{q_\xi} = \partial_{\mathbf{w}}\mathcal{K} = 0 \quad \text{even when} \quad \partial_\tau\alpha_{q_\xi} \neq 0\,,\ \partial_\xi\alpha_{q_\xi} \neq 0 \quad \text{and} \quad \partial_\tau\mathcal{K} \neq 0\,,\ \partial_\xi\mathcal{K} \neq 0$$

Under hypothesis 1 we can rewrite the spatial flux as

$$\mathbf{f} = \begin{bmatrix} \alpha_{q_\xi} w_2 \\ \alpha_{q_\xi}\dfrac{w_2^2}{w_1} + \beta\dfrac{w_1^2}{2} \end{bmatrix}$$

and evaluate its Jacobian with respect to the unknown $\mathbf{w}$ as

$$A = \frac{\partial\mathbf{f}}{\partial\mathbf{w}} = \begin{pmatrix} 0 & \alpha_{q_\xi} \\ \beta h - \alpha_{q_\xi}u^2 & 2\alpha_{q_\xi}u \end{pmatrix} \tag{17}$$

The matrix A is easily shown to have real eigenvalues and linearly independent eigenvectors. In particular, the eigenvalues of A are given by

$$\lambda_1 = q_\xi + \sqrt{\alpha_{q_\xi}\beta h}\,, \qquad \lambda_2 = q_\xi - \sqrt{\alpha_{q_\xi}\beta h} \tag{18}$$

Denoting by $c = \sqrt{\alpha_{q_\xi}\beta h} \geq 0$ the pseudo-speed of sound, the eigenmatrices of A are readily shown to be

$$R = (\mathbf{r}_1, \mathbf{r}_2) = \begin{pmatrix} \alpha_{q_\xi} & \alpha_{q_\xi} \\ \lambda_1 & \lambda_2 \end{pmatrix}, \qquad L = \begin{pmatrix} \mathbf{l}_1^T \\ \mathbf{l}_2^T \end{pmatrix} = \frac{1}{2c} \begin{pmatrix} -\dfrac{\lambda_2}{\alpha_{q_\xi}} & 1 \\ \dfrac{\lambda_1}{\alpha_{q_\xi}} & -1 \end{pmatrix} \tag{19}$$

where ^{T} denotes the transpose of a matrix. As usual we have $A = R\,\mathrm{diag}\,(\lambda)\,L$. Note that the matrix A is not enough to determine the quasi-linear form of the system, which has to take into account the dependence of α_{q_ξ} and $\mathcal{K}$ on τ and ξ. In particular, the quasi-linear of (14) reads :

$$\partial_\tau \mathbf{w} + A\partial_\xi \mathbf{w} = \mathbf{\Sigma} - \begin{pmatrix} hu & 0 \\ h(u^2 - \beta h\cos\theta) & \dfrac{h^2\cos^2\theta}{2} \end{pmatrix} \partial_\xi \begin{pmatrix} \alpha_{q_\xi} \\ \mathcal{K} \end{pmatrix} \tag{20}$$

In non-compact form the last equations can also be rewriten by regrouping terms so that the steady balance associated to the lake at rest state is easily put in evidence :

$$\begin{aligned} &\partial_\tau(hu) - \alpha_{q_\xi} u^2 \partial_\xi h + 2\alpha_{q_\xi} u \partial_\xi(hu) + h\cos\theta\partial_\xi\left(\mathcal{K}h\cos\theta + b\right) \\ &\quad + hu^2\partial_\xi\alpha_{q_\xi} - \frac{h^2\cos^2\theta}{2}\partial_\xi\mathcal{K} \\ &\quad + \alpha_\rho u\partial_\tau b + \mathcal{N}\mathrm{sign}(u)\cos^2\theta = 0 \end{aligned} \tag{21}$$

We can now clearly see that at steady state, for constant $u = 0$ hence constant $\mathcal{K} = \mathcal{K}_0$ we obtain the condition $\partial_\xi\left(\mathcal{K}_0 h\cos\theta + b\right) = 0$. In the following we will denote by $\eta^{\mathcal{K}}$ the *pesudo*-free surface level

$$\eta^{\mathcal{K}} = \mathcal{K}h\cos\theta + b \tag{22}$$

4.2. **Energy and symmetric quasi-linear form**

In order to derive an energy inequality for the system, we proceed by steps of increasing complexity. Let us first consider a very simplified case in which both α_{q_ξ} and $\mathcal{K}$ are frozen. In this case we shall speak of *frozen coefficients assumption*, and *frozen coefficients system.*

The following result holds for the frozen coefficient system.

Proposition 2. In the the frozen coefficients case $\alpha_{q_\xi} = c_1 = c^t$, $\mathcal{K} = c_2 = c^t$, system (14) is endowed with an entropy pair given by the total energy E with corresponding energy flux f^E

$$E = h\cos\theta\left(\frac{{q_\xi}^2}{2} + \mathcal{K}\frac{h\cos\theta}{2} + b\right), \quad f^E = q_\xi h\cos\theta\left(\frac{{q_\xi}^2}{2} + \mathcal{K}h\cos\theta + b\right) = q_\xi h\cos\theta\left(\frac{{q_\xi}^2}{2} + \eta^{\mathcal{K}}\right) \tag{23}$$

The energy E is convex, it symmetrizes the system, and it verifies the inequality

$$\partial_\tau E + \partial_\xi f^E \leq \mathcal{S}^E = \cos\theta\left[(h - \alpha_\rho(\eta^{\mathcal{K}} + \frac{{q_\xi}^2}{2})\right]\partial_\tau b - \mathcal{N}h|u|\cos\theta \tag{24}$$

In the particular case $\alpha = 1$, and for a flat basal surface (that is $b = c^t$ in space and time), and $\mathcal{K} = 1$, we recover the standard shallow water entropy inequality with gravity $g = 1$.

$$\partial_t \left(h\frac{u^2}{2} + \frac{h^2}{2} \right) + \partial_x \left(hu\frac{u^2}{2} + u\frac{h^2}{2} \right) + \partial_x \left(u\frac{h^2}{2} \right) \leq -\mathcal{N}h|u|$$

Proof. In order to verify all the properties we start by introducing the vector of symmetrizing variables $\mathbf{v}$

$$\mathbf{v} = \begin{pmatrix} \partial_h E \\ \partial_{hu} E \end{pmatrix} = \begin{pmatrix} \beta h - \dfrac{q_\xi u}{2} + b\cos\theta \\ q_\xi \end{pmatrix} \tag{25}$$

Straightforward calculations show that

$$A_0 = \frac{\partial \mathbf{w}}{\partial \mathbf{v}} = \frac{1}{\alpha_{q_\xi}\beta} \begin{pmatrix} \alpha & q_\xi \\ q_\xi & q_\xi u + \beta h \end{pmatrix} \tag{26}$$

For the energy E to be convex, A_0 must be positive definite. This is readily shown by noting that $\forall X = (x_1,\, x_2) \in \mathbf{R}^2$

$$X\, A_0\, X^T = \alpha_{q_\xi}(x_1 + u x_2)^2 + \beta h x_2^2 > 0$$

We can also easily show that A_0 is a right symmetrizer for the Jacobian A (cf. equation (17)) :

$$\frac{\partial \mathbf{f}}{\partial \mathbf{v}} = A_1 = AA_0 = \frac{1}{\alpha_{q_\xi}\beta} \begin{pmatrix} \alpha_{q_\xi}^2 u & {q_\xi}^2 + \alpha\beta h \\ {q_\xi}^2 + \alpha\beta h & (3\beta h + q_\xi u) q_\xi \end{pmatrix} \tag{27}$$

For a smooth flow, the energy equation is readily obtained as

$$\mathbf{v}^T \left(\partial_\tau \mathbf{w} + \partial_\xi \mathbf{f} - \mathbf{\Sigma} \right) = 0$$

which can be shown by simple manipulations to reduce exactly to (24) with definitions (23) of the energy and energy flux respectively. For non-smooth solutions, this equation reduces to inequality (24).

The last property is easily found by neglecting the temporal and spatial derivatives of b, and using the fact that $cos\theta = 1$, hence $\xi = x$, and $\tau = t$. □

A more general result is obtained by using hypothesis 1, hence taking into account the variation of the basal surface, and of the model parameter $\mathcal{K}$.

Proposition 3. Under hypothesis 1, system (14) is endowed with an entropy pair given by the total energy with corresponding energy flux (23). The energy E is convex, it symmetrizes the system, and it verifies the inequality

$$\begin{gathered} \partial_\tau E + \partial_\xi f^E \leq \mathcal{S}^E + \sigma^E \\ \sigma^E = h\left(\frac{u^2}{2} - \eta^{\mathcal{K}} \cos^2\theta \right) \left(\partial_\tau \alpha_{q_\xi} + q_\xi \partial_\xi \alpha_{q_\xi} \right) + \frac{h^2 \cos^2\theta}{2} \left(\partial_\tau \mathcal{K} + \partial_\xi \mathcal{K} \right) \end{gathered} \tag{28}$$

with $\mathcal{S}^E$ as in (24). In the particular case $\alpha = 1$, and for a flat basal surface (that is $b = c^t$ in space and time), and $\mathcal{K} = 1$, we recover the standard shallow water entropy inequality with gravity $g = 1$

$$\partial_t \left(h\frac{u^2}{2} + \frac{h^2}{2} \right) + \partial_x \left(hu\frac{u^2}{2} + u\frac{h^2}{2} \right) + \partial_x \left(u\frac{h^2}{2} \right) \leq -\mathcal{N}h|u|$$

Proof. Due to hypothesis 1 all the Jacobian computations remain unchanged. This implies that the vector of symmetrizing variables $\mathbf{v}$ is still defined by (25), and the Jacobian of the variable transformation is still given by (26), which is symmetric and positive definite (as long as $\alpha_{q_\xi},\, \beta \geq 0$). Moreover, A_0 is a right symmmetrizer of the Jacobian A (equation (17)). Lastly, the energy balance is readily obtained as

$$\mathbf{v}^T \left(\partial_\tau \mathbf{w} + \partial_\xi \mathbf{f} - \mathbf{\Sigma}\right) = 0$$

which leads to (28) after some lengthy calculations. The last property is easily found by neglecting the temporal and spatial derivatives of b, α_{q_ξ}, and $\mathcal{K}$, and using the fact that $\cos\theta = 1$, hence $\xi = x$, and $\tau = t$. □

5. Numerical approximation : Finite volume

In this section we discuss a family of numerical treatments of the source term $\mathbf{\Sigma}$ that guarantee the exact preservation of the steady lake at rest solution of proposition 1. These schemes can be generally written as

$$\frac{\delta \mathbf{w}_i^n}{\delta\tau}\delta\xi_i^n + \mathbf{\Phi}^c_{i+\frac{1}{2}} - \mathbf{\Phi}^c_{i-\frac{1}{2}} + \delta\mathbf{\Phi}_{i+\frac{1}{2}} + \delta\mathbf{\Phi}_{i-\frac{1}{2}} + \mathbf{\Phi}^{\mathbf{\Sigma}}_{i-\frac{1}{2}} + \mathbf{\Phi}^{\mathbf{\Sigma}}_{i+\frac{1}{2}} = 0 \tag{29}$$

where $\mathbf{\Phi}^c_{i\pm\frac{1}{2}} = \mathbf{\Phi}^c_{i\pm\frac{1}{2}}(\mathbf{w}^L_{i\pm\frac{1}{2}},\, \mathbf{w}^R_{i\pm\frac{1}{2}})$ represents the centered flux

$$\mathbf{\Phi}^c_{i\pm\frac{1}{2}}(\mathbf{w}^L_{i\pm\frac{1}{2}},\, \mathbf{w}^R_{i\pm\frac{1}{2}}) = \frac{\mathbf{f}(\mathbf{w}^R_{i\pm\frac{1}{2}}) + \mathbf{f}(\mathbf{w}^L_{i\pm\frac{1}{2}})}{2} \tag{30}$$

The terms $\delta\mathbf{\Phi}_{i\pm\frac{1}{2}}$ are the terms corresponding to the Finite Volume stabilization, while the additional fluxes $\mathbf{\Phi}^{\mathbf{\Sigma}}_{i\pm\frac{1}{2}}$ represent the contribution of the source term. The stabilization terms are written in the following general form

$$\delta\mathbf{\Phi}_{i\pm\frac{1}{2}}(\mathbf{w}^L_{i\pm\frac{1}{2}},\, \mathbf{w}^R_{i\pm\frac{1}{2}}) = \mp\frac{\tau_{i\pm\frac{1}{2}} A^{i\pm\frac{1}{2}}}{\delta\xi^n_{i\pm\frac{1}{2}}}\left(\mathbf{f}(\mathbf{w}^R_{i\pm\frac{1}{2}}) - \mathbf{f}(\mathbf{w}^L_{i\pm\frac{1}{2}})\right) \tag{31}$$

where

$$A^{i\pm\frac{1}{2}} = A\left(\frac{\mathbf{w}^L_{i\pm\frac{1}{2}} + \mathbf{w}^R_{i\pm\frac{1}{2}}}{2}\right)$$

Definition (31) is inspired from finite element SUPG like discretizations (or equivalently residual distribution schemes) and it basically represents a crude approximation of integrals of the type

$$\delta\mathbf{\Phi}_{i\pm\frac{1}{2}} = \mp\tau_{i\pm\frac{1}{2}} \int_{i\pm1}^{i} \frac{\partial \mathbf{f}}{\partial \mathbf{w}} \partial_\xi\varphi_i \partial_\xi \mathbf{f}\; d\xi$$

with φ_i the i-th element of a given set of basis functions. The term (31) encompasses several finite volume stabilization operators, depending on the choice of the local time scale $\tau_{i\pm\frac{1}{2}}$. For example, a Lax-Wendroff stabilization is obtained with the choice

$$\tau_{i\pm\frac{1}{2}} = \tau_{LW} = \frac{\delta\tau}{2} \tag{32}$$

A conservative upwind flux splitting is instead obtained if

$$\tau_{i\pm\frac{1}{2}} = \frac{\delta\xi^n_{i\pm\frac{1}{2}}}{2}|A^{i\pm\frac{1}{2}}|^{-1} \tag{33}$$

where the absolute value of the matrix A is obtained as usual via eigenvalue decomposition, and

$$\delta\xi^n_{i\pm\frac{1}{2}} = \pm(\xi^n_{i\pm1} - \xi^n_i)$$

The source term fluxes are obtained in a similar way. In order to mimic the treatment of the derivatives of the flux, the idea is to look for approximations of the type

$$\mathbf{\Phi}^{\mathbf{\Sigma}}_{i\pm\frac{1}{2}} = \mp\frac{1}{2}\int_{i\pm1}^{i} \mathbf{\Sigma}\, d\xi \mp \tau_{i\pm\frac{1}{2}} \int_{i\pm1}^{i} \frac{\partial \mathbf{f}}{\partial \mathbf{w}} \partial_\xi \varphi_i \mathbf{\Sigma}\, d\xi = \mp\left(\frac{1}{2} \mp \frac{\tau_{i\pm\frac{1}{2}} A^{i\pm\frac{1}{2}}}{\delta\xi^n_{i\pm\frac{1}{2}}}\right) \int_{i\pm1}^{i} \mathbf{\Sigma}\, d\xi$$

Depending on the hypotheses made on the spatial variation of $\mathbf{\Sigma}$ different formulas can be obtained. For clarity, in the following we focus on source terms that can be decomposed as

$$\mathbf{\Sigma} = m(\mathbf{w},\tau,\xi)\partial_\xi g(\mathbf{w},\tau,\xi) + l(\mathbf{w},\tau,\xi)$$

for some known functionals $m(\mathbf{w},\tau,\xi)$, $g(\mathbf{w},\tau,\xi)$, and $l(\mathbf{w},\tau,\xi)$. For our model for example we have (in absence of deposition/erosion)

$$m = \begin{pmatrix} 0 \\ h\cos\theta \end{pmatrix}, \quad g = \begin{pmatrix} 0 \\ b \end{pmatrix}, \quad l = \begin{pmatrix} 0 \\ \mathcal{N}\text{sign}(u)\cos^2\theta \end{pmatrix}$$

Three different cases can be considered : a discontinuous piecewise constant approximation of $\mathbf{\Sigma}$, a discontinuous piecewise linear approximation of $\mathbf{\Sigma}$, and a continuous piecewise linear approximation. Let us focus on the last case which gives

$$\int_{i\pm1}^{i} \mathbf{\Sigma}\, d\xi \approx \overline{m}\,(g_i - g_{i\pm1}) \mp \overline{l}\delta\xi^n_{i\pm\frac{1}{2}}, \quad \overline{()} = \frac{()_i + ()_{i\pm1}}{2}$$

This leads for our model (no erosion/deposition) to the following source term flux.

$$\mathbf{\Phi}^{\mathbf{\Sigma}}_{i\pm\frac{1}{2}} = \left(\frac{1}{2} \mp \frac{\tau_{i\pm\frac{1}{2}} A^{i\pm\frac{1}{2}}}{\delta\xi^n_{i\pm\frac{1}{2}}}\right)\left(\begin{pmatrix} 0 \\ \overline{h\cos\theta}\delta b_{i\pm\frac{1}{2}} \end{pmatrix} + \delta\xi^n_{i\pm\frac{1}{2}} \begin{pmatrix} 0 \\ \mathcal{N}\text{sign}(u)\cos^2\theta \end{pmatrix}\right) \tag{34}$$

$$\text{with} \quad \delta b_{i\pm\frac{1}{2}} = \pm\,(b_{i\pm1} - b_i)$$

With these definitions, we have the following property.

Proposition 4. In absence of deposition/erosion, the first order scheme given by (29) with definitions (30), (31), and (34) of the centered, stabilizing, and source flux respectively, using a piecewise constant approximation for the evaluation of the spatial fluxes, preserves exactly the steady lake at rest type solution of proposition 1.

Proof. To achieve the proof, we suppose to be given an initial solution that verifies in each cell

$$\eta^{\mathcal{K}}_i = \mathcal{K}_0 h_i \cos\theta_i + b_i = \eta^* \quad \forall\, i$$

with $u = 0$ everywhere. This leads to

$$\overline{h\cos\theta}\delta b_{i\pm\frac{1}{2}} - \mathcal{K}_0\overline{h\cos\theta}\,\delta(h\cos\theta)_{i\pm\frac{1}{2}} = -\delta\big(\mathcal{K}_0 h^2\cos^2\theta\big)_{i\pm\frac{1}{2}} \tag{35}$$

with

$$\delta\big(\mathcal{K}_0 h^2\cos^2\theta\big)_{i\pm\frac{1}{2}} = \pm\left(\big(\mathcal{K}_0 h^2\cos^2\theta\big)_{i\pm1} - \big(\mathcal{K}_0 h^2\cos^2\theta\big)_i\right)$$

Obviously, due to the condition $u = 0$ the contribution of the friction term vanishes identically, so that (35) is the only entry in the source term integral.

We now consider the spatial fluxes. For the given initial state we have

$$\mathbf{f}^L_{i+\frac{1}{2}} = \mathbf{f}^R_{i-\frac{1}{2}} = \begin{pmatrix} 0 \\ \left(\mathcal{K}_0 h^2 \cos^2\theta\right)_i \end{pmatrix}, \quad \mathbf{f}^R_{i+\frac{1}{2}} = \begin{pmatrix} 0 \\ \left(\mathcal{K}_0 h^2 \cos^2\theta\right)_{i+1} \end{pmatrix}, \quad \mathbf{f}^L_{i-\frac{1}{2}} = \begin{pmatrix} 0 \\ \left(\mathcal{K}_0 h^2 \cos^2\theta\right)_{i-1} \end{pmatrix}$$

These expressions, combined with (35) immediately show that

$$\delta\mathbf{\Phi}_{i\pm\frac{1}{2}} \mp \frac{\tau_{i\pm\frac{1}{2}} A^{i\pm\frac{1}{2}}}{\delta\xi^n_{i\pm\frac{1}{2}}} \begin{pmatrix} 0 \\ h\cos\theta\delta b_{i\pm\frac{1}{2}} \end{pmatrix} = \mp \frac{\tau_{i\pm\frac{1}{2}} A^{i\pm\frac{1}{2}}}{\delta\xi^n_{i\pm\frac{1}{2}}} \begin{pmatrix} 0 \\ \delta\left(\mathcal{K}_0 h^2 \cos^2\theta\right)_{i\pm\frac{1}{2}} - \delta\left(\mathcal{K}_0 h^2 \cos^2\theta\right)_{i\pm\frac{1}{2}} \end{pmatrix} = 0$$

Hence scheme (29) reduces to

$$\frac{\delta\mathbf{w}^n_i}{\delta\tau}\delta\xi^n_i + \mathbf{\Phi}^c_{i+\frac{1}{2}} - \mathbf{\Phi}^c_{i-\frac{1}{2}} - \frac{1}{2}\begin{pmatrix} 0 \\ \delta\left(\mathcal{K}_0 h^2 \cos^2\theta\right)_{i+\frac{1}{2}} \end{pmatrix} - \frac{1}{2}\begin{pmatrix} 0 \\ \delta\left(\mathcal{K}_0 h^2 \cos^2\theta\right)_{i-\frac{1}{2}} \end{pmatrix} = 0$$

Straight forward calculations show that last expression reduces to

$$\delta h^n_i = 0$$
$$2\frac{\delta\xi^n_i}{\delta\tau}\delta(hu)^n_i = \left(\mathcal{K}_0 h^2 \cos^2\theta\right)^R_{i-\frac{1}{2}} - \left(\mathcal{K}_0 h^2 \cos^2\theta\right)^L_{i+\frac{1}{2}} = 0$$

having used the expressions of the fluxes given earlier. This achieves the proof. □

The reader is referred to [23] for a similar construction for the shallow water equations.

5.1. **Conservation during erosion/deposition**

During erosion/deposition process, the mass and the momentum are conserved. That is

$$\rho_d\partial_\tau\mathcal{D} = \rho_s\partial_\tau\mathcal{V} \Longrightarrow \partial_\tau\mathcal{D} = \alpha_\rho\partial_\tau\mathcal{V} \quad \textit{and} \quad \rho_d\partial_\tau(\mathcal{D}u) = 0$$

where ρ_d and $\mathcal{D}$ (resp. ρ_s and $\mathcal{V}$) are the density and the volume of the moving component (resp. static component), u is the velocity of the moving frame.

In practice, the evolution of topography is defined by a set of coordinates $x_{i+\frac{1}{2}} \equiv x_{i+\frac{1}{2}}(\tau)$ and angles $\theta_{i+\frac{1}{2}} \equiv \theta_{i+\frac{1}{2}}(\tau)$ localized at the cell interface. The moving frame is associated to the set of height $h_i \equiv h_i(\tau)$, velocities $u_i \equiv u_i(\tau)$ and angles $\theta_i \equiv \theta_i(\tau)$ centered on cells. From the angle θ_i a local normal $\boldsymbol{\eta}_i \equiv \boldsymbol{\eta}(\theta_i)$ to the interface is defined.

$$\mathcal{D}_i \simeq \mathcal{D}\left(x_{i+\frac{1}{2}}, x_{i-\frac{1}{2}}, h_i, \theta_i\right), \quad \mathcal{V}_i \simeq \mathcal{V}\left(x_{i+\frac{1}{2}}, x_{i-\frac{1}{2}}\right)$$

At the discrete level, conservation of the mass can be formulated as:

$$\mathcal{D}^{n+1}_i = \mathcal{D}^n_i + \alpha_\rho\left(\delta\mathcal{V}\right)^{n,n+1}_i$$

where

$$\left(\delta\mathcal{V}\right)^{n,n+1}_i = \mathcal{Q}\left(x^n_{i+\frac{1}{2}}, x^{n+1}_{i+\frac{1}{2}}, x^{n+1}_{i-\frac{1}{2}}, x^n_{i-\frac{1}{2}}\right)$$
$$\left(\mathcal{D}\right)^n_i = \mathcal{Q}\left(x^n_{i+\frac{1}{2}}, x^{n*}_{i+\frac{1}{2}}, x^{n*}_{i-\frac{1}{2}}, x^n_{i-\frac{1}{2}}\right) = h^n_i\left(\delta\mathcal{D}\right)^n_i$$

with

$$x^{n*}_{i\pm\frac{1}{2}} = x^n_{i\pm\frac{1}{2}} + h^n_i \boldsymbol{\eta}^n_i \quad \textit{and} \quad (\delta\mathcal{D})^n_i = \frac{1}{2}\left(\boldsymbol{\eta}^n_i \wedge \left(x^n_{i+\frac{1}{2}} - x^n_{i-\frac{1}{2}}\right)\right)\boldsymbol{k}$$

Therefore, mass conservation is locally satisfied when

$$h^{n+1}_i = \frac{h^n_i\,(\delta\mathcal{D})^n_i + \alpha_\rho\,(\delta\mathcal{V})^{n,n+1}_i}{(\delta\mathcal{D})^{n+1}_i}$$

This means that, once $x^{n+1}_{i+\frac{1}{2}}$ and $\theta^{n+1}_{i+\frac{1}{2}}$ have been computed, the evolution of the interface should be approximated as

$$(\alpha_\rho\,\partial_t\mathcal{B})^{n,n+1}_i \simeq \frac{h^n_i\left((\delta\mathcal{D})^{n+1}_i - (\delta\mathcal{D})^n_i\right) - \alpha_\rho\,(\delta\mathcal{V})^{n,n+1}_i}{(\delta\mathcal{D})^{n+1}_i}$$

For momentum conservation we have

$$\mathcal{D}^{n+1}_i u^{n+1}_i = \mathcal{D}^n_i u^n_i \Longrightarrow h^{n+1}_i u^{n+1}_i = \frac{(\delta\mathcal{D})^n_i}{(\delta\mathcal{D})^{n+1}_i} h^n_i u^n_i$$

Therefore

$$(\alpha_\rho u\,\partial_t\mathcal{B})^{n,n+1}_i \simeq \frac{\left((\delta\mathcal{D})^{n+1}_i - (\delta\mathcal{D})^n_i\right)}{(\delta\mathcal{D})^{n+1}_i} h^n_i u^n_i$$

These approximations ensure that the discrete mass and momentum are conserved during the deposition/erosion process. However, this strategy can be applied only if we have already have $x^{n+1}_{i+\frac{1}{2}}$ and θ^{n+1}_i. This is achieved by considering the equation

$$\partial_\tau x = -(\theta - \Theta_n)\mathcal{E}(h,u,\theta)\boldsymbol{\eta}(\theta)$$

$$x^{n+1}_{i+\frac{1}{2}} = x^n_{i+\frac{1}{2}} - \delta\tau \frac{\displaystyle\sum_{j\in\vartheta(i+\frac{1}{2})} \zeta_j\left(\theta^n_j - \Theta_n\right)\mathcal{E}\left(h^n_j, u^n_j, \theta^n_j\right)\boldsymbol{\eta}(\theta^n_j)}{\displaystyle\sum_{j\in\vartheta(i+\frac{1}{2})}\zeta_j}$$

$$\theta^{n+1}_i = \frac{\zeta_0\theta^n_i + \displaystyle\sum_{j\in\vartheta(i)} \zeta_j\theta\left(x^{n+1}_{j-\frac{1}{2}}, x^{n+1}_{j+\frac{1}{2}}\right)}{\zeta_0 + \displaystyle\sum_{j\in\vartheta(i)}\zeta_j}$$

The strategy for erosion deposition is then complete.

5.2. **Numerical results**

5.2.1. *Granular column collapse.*

In this section we investigate numerically the spreading of dry granular column suddenly released on a horizontal plane. The initial flow and basal surfaces, are defined by:

$$b_0(x) = \ 5\ 10^{-2}\exp\left[-\left(\frac{x-3}{0.73}\right)^2\right], \quad \mathcal{T}(x) = 2\exp\left[-\left(\frac{x-3}{0.75}\right)^4\right],$$

with a dimensionless coordinate x. From the initial basal surface $b_0(x)$, we can compute the the inclination angle $\theta(x) \equiv \theta(\xi)$ and the associated normal $\boldsymbol{n}(x) \equiv \boldsymbol{n}(\xi)$. The point $\boldsymbol{x}(\xi) = (x, b_0(x))$ and its normal $\boldsymbol{n}(\xi)$ define a straight line that intersects with the curve $\mathcal{T}(x)$ at a point $\boldsymbol{x}_*(\xi) = (x_*, \mathcal{T}(x_*))$. Therefore, we have the initial

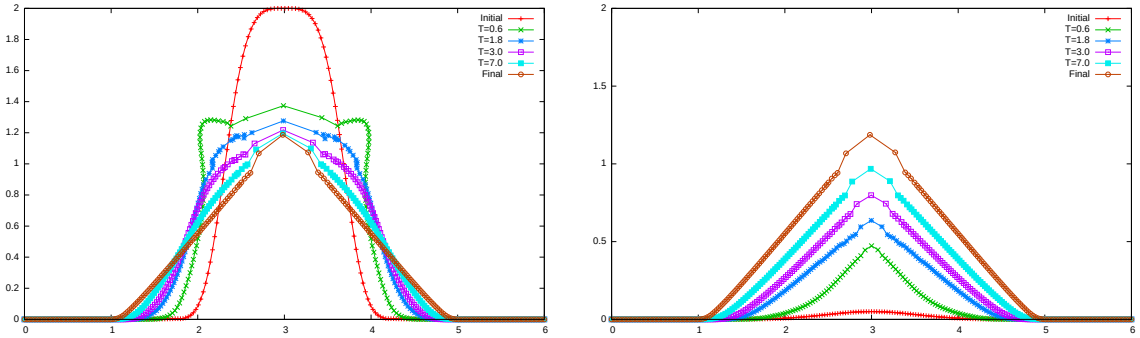

FIGURE 4. Evolution of the flow surface (left) and corresponding moving basal surface Plots at different dimensionless time units. At the final time $T = 100$ we have $h \leq 10^{-8}$.

depth $h(\xi) = \|\boldsymbol{x}_*(\xi) - \boldsymbol{x}(\xi)\|$. The erosion/deposition rate is given by Eq. (13) and the relevant parameters are $(\alpha_e,\, \alpha_v,\, e_\alpha) = (2.0,\, 1.0,\, 20)$. The other parameters of the computation are:

$$\theta_n = 35^\circ, \quad \delta = 23^\circ, \quad \phi = 34^\circ, \quad \alpha_\rho = 0.9, \quad \alpha_h = 0.05.$$

As the flowing layer has less density then that of the stagnant base, the basal friction coeficient is slightly lowered as $\mu = \tan 33^\circ$. Numerical results are obtained with 201 meshes and a seond order (space and time) method combined with a minmod limiter is used.

Figure 4 illustrates the simulated process of the basal surface moving upwards from the horizontal plane. The left panel shows the evolution of the free surface of the collapsing column and the right panel sketches the moving interface between flowing layer and stagnant base.

6. Concluding remarks

The present work is concerned with the complex granular flows, of which the deposition and erosion are significant. Experiments of granular column collapse demonstrate the both processes. The erodible model, proposed by Tai and Kuo [18] is used to describe the relevant phenomena. A well balanced numerical scheme for this model is developed, and the eigenstructure of its quasilinear form as well as the entropy inequality are assessed. Numerical application is performed to column collapse . When the initial basal surface is horizontal, one observes its upward movement during the collapse. The final surface inclination angle is slightly less than the angle of respose of the material.

However, not all the details observed experimentally are reproduced. At the first stage, the granular column collapse is quite fast, and the erosion process takes place at the interface between the surface flow and the resting bed until it reaches the vicinity of the internal stagnant core. Then the granular mass spreads on its flanks, producing the wedge deposit and the basal interface moves upwards. This indicates the future research topics of interest:

- Quantitative experimental measurement is to be collected for validation.
- The erosion mechanism needs to be re-examined extensively.
- A mesh smoothing technique is necessary to be able to capture the convergent motion near the top of the granular column.

Results on these ongoing research topics will be reported in subsequent publications.

References

[1] S. B. Savage and K. Hutter, "The motion of a finite mass of granular material down a rough incline." J. Fluid Mech. **199**, 177 (1989).

[2] S. P. Pudasaini and K. Hutter, "*Avalanche Dynamics*." Springer, Berlin, 2007.

[3] J.-P. Bouchaud, M. E. Cates, J. Ravi Prakash and S. F. Edwards, "A model for the dynamics of sandpile surfaces." J. Phys. I (France) **4**, 1383 (1994).

[4] F. Bouchut, E. D. Fernándes-Nieto, A. Mangeney and P. Y. Lagrée, "On new erosion models of Savage-Hutter type for avalanches." Acta Mech. **199**, 181 (2008).

[5] W. H. Hui, P. Y. Li and Z. W. Li, "A Unified Coordinate System for Solving the Two-Dimensional Euler Equations." J. Comput. Phys. **153**, 596 (1999).

[6] W. H. Hui and S. Koudriakov, "Computation of the shallow water equations using the unified coordinates." SIAM J. Sci. Comput. **23**, 1615 (2002).

[7] W. H. Hui, "A unified coordinates approach to computational fluid dynamics." J. Comp. and Applied Math. **163**, 15 (2004).

[8] W. H. Hui, "The unified coordinate system in computational fluid dynamics." Commun. Comput. Phys. **2**, 577 (2007).

[9] B. Andreotti, A. Daerr and S. Douady, "Scaling laws in granular flows down a rough plane." Phys. Fluids **14**, 415 (2002).

[10] A. Mangeney-Castelnau, F. Bouchut, J.P. Vilotte, E. Lajeunesse, A. Aubertin and Pirulli M., "On the use of Saint-Venant equations to simulate the spreading columns." J. Geophys. Res. **110** (2005).

[11] E. Lajeunesse, A. Mangeney-Castelnau and J.P. Vilotte, "Spreading of a Granular Mass on a Horizontal plane." Phys. Fluids, **16**(7), 2371–2381..

[12] G. Lube, H. E. Huppert, R.S.J. Sparks and M. Hallworth, "Axisymmetric Collapses of Granular Columns." J. Fluid Mech., **508**, 175–199..

[13] G. Lube, H.E. Huppert, R.S.J. Sparks and A. Freundt, "Collapses of two-dimensional granular columns." Phys. Rev. E, **72**, 041301..

[14] N.J. Balmforth and R.P. Kerswell, "Granular collapses in two dimensions." J. Fluid Mech., **538**, 399-428..

[15] E.L. Thompson and H.E. Huppert, "Granular column Collapses: further Experimental Results." J. Fluid Mech., **575**, 177-186..

[16] L. Staron and E.J. Hinch, "Study of the collapse of granular columns using two dimensional discrete-grain simulation. " J. Fluid Mech., **545**, 1-27..

[17] A. Mangeney, L. Staron, D. Volfson and L. Tsimring, "Comparison between discrete and continuum modeling of granular spreading." WSEAS Transactions on Mathematics, **2**(6), 373-380..

[18] Y.C. Tai and C.Y. Kuo, "A new model of granular flows over general topography with erosion and deposition." Acta Mech. **199**, 71–96 (2008).

[19] Y.C. Tai and Y.C. Lin, "A focused view of the behavior of granular flows down a confined inclined chute into horizontal run-out zone." Phys. Fluids **20**, 123302 (2008).

[20] F. Bouchut and M. Westdickenberg, "Gravity driven shallow water models for arbitrary topography." Commun. Math. Sci. **2**, 359 (2004).

[21] T.S. Komatsu, S. Inagaki, N. Nakagawa, S. Nasuno, "Creep Motion in a Granular Pile Exhibiting Steady Surface Flow." Phys. Rev. Lett., **86**, 1757–1760.

[22] Y.C. Tai, C.H. Chen, J.Y. Lan, K.C. Chen, C.Y. Kuo, "Internal Structure of a Finite Granular Mass Spreading on a Horizontal Plane." Cross-Strait Workshop on Engineering Mechanics 2008, September, 2008, Tainan/Taipei, Taiwan..

[23] M.E. Hubbard, P.Garcia-Navarro, "Flux Difference Splitting and the Balancing of Source Terms and Flux Gradients" J. of Comput. Phys., **165**-1, 89–125 (2000).